

---

# Reverse the auditory processing pathway: Coarse-to-fine audio reconstruction from fMRI

---

Che Liu<sup>1,2,3\*</sup>, Changde Du<sup>1,2\*</sup>, Xiaoyu Chen<sup>1,2</sup>, Huiguang He<sup>1,2,3†</sup>

<sup>1</sup>Key Laboratory of Brain Cognition and Brain-inspired Intelligence Technology

<sup>2</sup>State Key Laboratory of Multimodal Artificial Intelligence Systems, CASIA, Beijing, China

<sup>3</sup>School of Future Technology, University of Chinese Academy of Sciences  
{liuche2022, changde.du, chenxiaoyu2022, huiguang.he}@ia.ac.cn

## Abstract

Drawing inspiration from the hierarchical processing of the human auditory system, which transforms sound from low-level acoustic features to high-level semantic understanding, we introduce a novel coarse-to-fine audio reconstruction method. Leveraging non-invasive functional Magnetic Resonance Imaging (fMRI) data, our approach mimics the inverse pathway of auditory processing. Initially, we utilize CLAP to decode fMRI data coarsely into a low-dimensional semantic space, followed by a fine-grained decoding into the high-dimensional AudioMAE latent space guided by semantic features. These fine-grained neural features serve as conditions for audio reconstruction through a Latent Diffusion Model (LDM). Validation on three public fMRI datasets—Brain2Sound, Brain2Music, and Brain2Speech—underscores the superiority of our coarse-to-fine decoding method over stand-alone fine-grained approaches, showcasing state-of-the-art performance in metrics like FD, FAD, and KL. Moreover, by employing semantic prompts during decoding, we enhance the quality of reconstructed audio when semantic features are suboptimal. The demonstrated versatility of our model across diverse stimuli highlights its potential as a universal brain-to-audio framework. This research contributes to the comprehension of the human auditory system, pushing boundaries in neural decoding and audio reconstruction methodologies.

## 1 Introduction

Hearing is one of the most important senses for humans, responsible for receiving external auditory stimuli and transmitting the information to the brain for processing and understanding. Researchers aim to explore the auditory perception mechanisms of the human brain from the fields of both neuroscience and computer science [1–5]. A key goal is to decode neural information from the human brain and reconstruct the original stimuli. The common brain-to-audio reconstruction tasks can be categorized into *brain-to-sound* task [6, 7] for reconstructing all natural sounds in the environment, *brain-to-music* task [8–10] for the music, and *brain-to-speech* task [11–16] for the human voice, based on the different stimulus audios.

Some researchers first attempted to map brain signals to the spectrograms or mel-spectrograms of the stimulus audios using linear regression [8, 11–13]. Others introduce non-linear units and use simple networks such as MLP [8, 12, 13], BiLSTM [9, 14], Transformer [14], etc. This approach can restore the detailed temporal and frequency information of the spectrogram, but the reconstructed audio lacks semantic information, especially for non-invasive brain signals.

---

\*Equal contributions

†Huiguang He is the corresponding author.

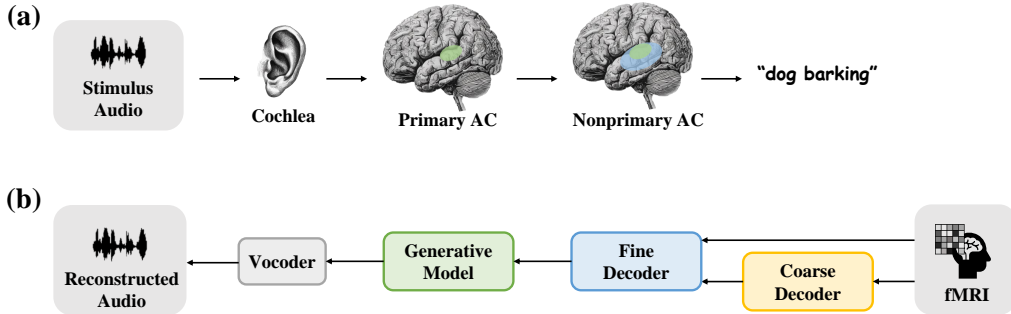


Figure 1: (a) The hierarchical auditory processing pathway of humans. The stimulus audio is gradually decomposed into time-frequency representation, low-level acoustic features, and high-level semantic characteristics. (b) The pipeline for our coarse-to-fine reconstruction from fMRI. Brain activity is decoded progressively into semantic, acoustic, and spectrogram levels, ultimately resulting in reconstructed audio.

As research progresses, researchers have found that Deep Neural Network (DNN) features are closer to neural responses in the human brain compared to artificial acoustic representations like spectrograms [1, 3, 4, 17, 18]. Therefore, researchers [7, 15, 16] first decode neural signals into DNN features as an intermediate representation and then use generative models to reconstruct the spectrogram. The intermediate representation is typically chosen from the intermediate layers of DNN, serving as high-dimensional fine-grained features that contain both semantic and acoustic information of sound. However, directly decoding these fine-grained features is often challenging and yields limited results, especially for non-invasive neural signals.

There are also works that decode neural signals coarsely into the low-dimensional semantic space. For example, Denk et al. [10] decodes neural signals into 128-dimensional MuLan embeddings and then predicts high-dimensional acoustic embeddings and generates music using MusicLM. However, this reconstruction model relies on the generative ability of MusicLM and cannot be transferred to audio forms other than music.

Let’s turn our focus back to neuroscience. As shown in Figure 1(a), research has indicated that in the cochlea and subcortical structures of the human ear, sound is decomposed into frequency-specific temporal patterns similar to spectrograms [4, 6, 19]. Further into the cerebral cortex, the human auditory system has two information processing pathways from low-level to high-level [20–24]. In recent years, an increasing amount of research has found that this cortical processing hierarchy aligns with the functional hierarchy of auditory DNN [1–4, 17, 18, 25]. The primary auditory cortex is more sensitive to shallow or intermediate DNN features, which represent low-level acoustic features, while the nonprimary auditory cortex is more sensitive to deep DNN features, which represent high-level semantic features.

Inspired by the acoustic-to-semantic stream, we model each physiological structure of the auditory processing pathway and propose an opposite coarse-to-fine audio reconstruction method, as shown in Figure 1(b). We use non-invasive fMRI as the neural signal. First, a coarse-to-fine brain decoding process is conducted. We decode fMRI data into the low-dimensional CLAP [26] space to obtain coarse-grained semantic features, and then under the guidance of these semantic features, we decode the fMRI data into the high-dimensional AudioMAE [27] latent space to obtain fine-grained acoustic features. Next, we use the decoded fine-grained neural features as conditions to reconstruct the mel-spectrogram using a Latent Diffusion Model (LDM) [28], and then restore the stimulus waveform using a Vocoder [29].

We validate our approach on three publicly available fMRI datasets: Brain2Sound, Brain2Music, and Brain2Speech. The results demonstrate that coarse-to-fine decoding outperforms directly fine-grained decoding in both details and semantics. Our method achieves state-of-the-art levels in metrics such as FD, FAD, and KL for the reconstructed audio across all three datasets.

Due to the complexity and diversity of sound signals, as well as the low resolution of neural signals [7], brain-to-audio decoding is generally considered challenging, especially in semantic decoding. Therefore, we attempt to provide the model with simple semantic prompts during decoding, such as the music genres or the genders of speakers. The experimental results demonstrate that

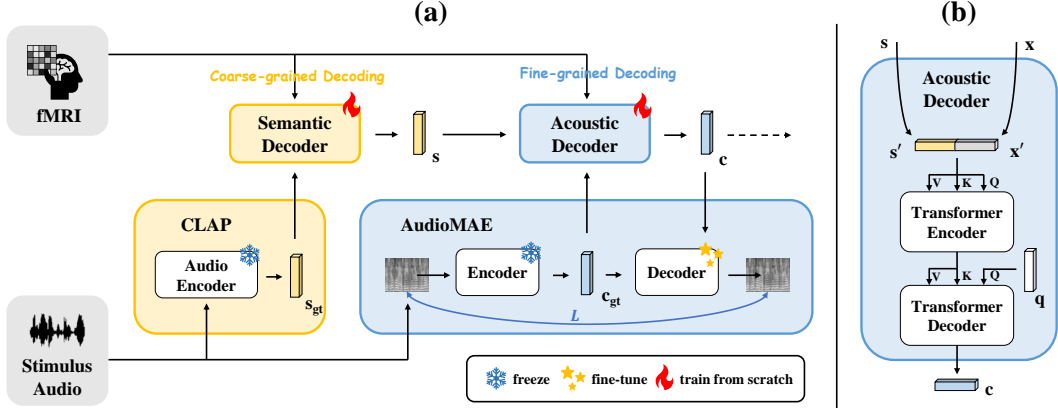


Figure 2: (a) Coarse-to-fine brain decoding. In the **coarse-grained decoding**, fMRI is decoded into the semantic space of CLAP. In the **fine-grained decoding**, fMRI is decoded into the acoustic space of AudioMAE. (b) Detailed structure of Acoustic Decoder.

providing prompts can improve the semantic quality of the reconstructed audio when the decoded semantic features are poor.

Our contributions are as follows: (1) We propose a coarse-to-fine neural decoding model and reconstruct high-quality waveforms with both semantic and detailed information. We also confirm that coarse-to-fine decoding is superior to solely fine-grained decoding. (2) Our model achieves good results on datasets with three different kinds of stimuli, demonstrating its strong transferability. It can serve as a universal brain-to-audio framework. (3) We attempt to provide semantic prompts and prove that they can enhance the reconstruction quality when semantic decoding is challenging.

## 2 Method

Let  $y \in \mathbb{R}^L$  represent an audio stimulus and  $x \in \mathbb{R}^V$  represent the corresponding fMRI signal, where  $L$  is the length of the audio samples and  $V$  is the number of voxels in  $x$ . The brain-to-audio reconstruction process can be formulated as  $\mathcal{R} : x \mapsto y$ . Our approach is to first decode an intermediate representation  $c$  from  $x$ , and then generate  $y$  using a generative model  $\mathcal{G}$  conditioned on  $c$ . To obtain the condition  $c$ , we follow a coarse-to-fine process. First, we perform a coarse-grained decoding by a Semantic Decoder  $\mathcal{D}^{Sem} : x \mapsto s$  to extract the semantic embedding  $s$  from fMRI. Then, we use a semantically-guided Acoustic Decoder  $\mathcal{D}^{Aco} : (s, x) \mapsto c$  to jointly decode the condition  $c$  with both semantics and acoustic details. After decoding, we use an LDM as the generative model  $\mathcal{G} : c \mapsto y$  to reconstruct the stimulus audio conditioned on  $c$ . We will introduce the coarse-grained decoding process of  $\mathcal{D}^{Sem}$  in Section 2.1.1, discuss the design of  $\mathcal{D}^{Aco}$  and the fine-grained decoding process in Section 2.1.2, and describe the training of  $\mathcal{G}$  in Section 2.2.

### 2.1 Coarse-to-fine brain decoding

#### 2.1.1 Coarse-grained semantic decoding

We use the CLAP feature as the coarse-grained semantic embedding of audio. CLAP, or contrastive language-audio pretraining [26], is a pretrained multi-modal model that aligns representations of audio with natural language descriptions. Pretrained on LAION-Audio-630K dataset [26] containing audios of human speech and song, natural sounds, and audio effects music, CLAP features are semantically aligned with various categories of audios, providing rich semantic information.

We model the Semantic Decoder  $\mathcal{D}^{Sem} : x \mapsto s$  as a ridge regression model. As shown in Figure 2, we firstly use CLAP’s Audio Encoder to extract the ground truth semantic feature of the stimulus audio  $y$ , denoted as  $s_{gt} \in \mathbb{R}^{512}$ . Then, we perform the L2-regularized linear regression from  $x$  to  $s_{gt}$  using PyFastL2LiR<sup>3</sup> toolkit, which provides fast ridge regression and voxel selection functionalities. For

<sup>3</sup><https://github.com/KamitaniLab/PyFastL2LiR>

each dimension of  $s_{gt}$ , we only select 500 voxels for regression based on the correlation coefficient. Thus, we obtain a sparse mapping matrix  $W \in \mathbb{R}^{V \times 512}$  and a bias  $b \in \mathbb{R}^{512}$ . The semantic embedding  $s$  of fMRI can be inferred by  $s = xW + b$  and  $s \in \mathbb{R}^{512}$ .

### 2.1.2 Fine-grained acoustic decoding

We use the AudioMAE latent feature as the fine-grained acoustic embedding of audio. AudioMAE, or audio mask autoencoder [27], is a self-supervised pretrained model, which consists of an encoder  $\mathcal{E}^A$  and a decoder  $\mathcal{D}^A$  and focuses on the reconstruction of the masked patches.

The reason we choose the AudioMAE latent embedding as the acoustic feature instead of other DNN features is threefold: (1) AudioMAE is trained on a generative task, which retains more low-level acoustic details compared to the discriminative models like VGGish-ish [30] used in Park et al. [7] and Wav2Vec 2.0 [31] used in Kim et al. [15]. (2) Compared to the normal autoencoder used in Chen et al. [16], AudioMAE performs a masked patch prediction task, which models the whole patches of the spectrogram. The empirical evidence [32] shows that this makes the AudioMAE feature space more inclined to cluster audio of the same category together compared to VAE, indicating that AudioMAE better preserves high-level semantic information. (3) Pretrained on AudioSet [33] which consists of natural sounds, human and animal sounds, and music, AudioMAE can work well in the general audio domain. In comparison, the MusicLM [34] used in Denk et al. [10] can only model the music domain. Taking all the points above into consideration, AudioMAE features are highly suitable for fine-grained features in our method, containing rich semantic and acoustic details.

As shown in Figure 2, we first transform the stimulus waveform  $y$  into 128 Kaldi [35]-compatible Mel-frequency bands with a 25ms Hanning window that shifts every 10 ms following AudioMAE [27], obtaining the mel-spectrogram  $m$ . Then we divide  $m$  into  $16 \times 16$  patches  $m^p \in \mathbb{R}^{N_{patch} \times 256}$  and encode the patches into  $c_{gt} = \mathcal{E}^A(m^p) \in \mathbb{R}^{N_{patch} \times 768}$  with no mask, where  $N_{patch}$  represents the number of patches. Then we decode  $c_{gt}$  into the reconstructed patches  $m_{upp}^p = \mathcal{D}^A(c_{gt})$  and unpatchify them into the mel-spectrogram  $m_{upp}$ . We consider  $c_{gt}$  as the ground truth acoustic feature of the stimulus audio  $y$  and  $m_{upp}$  as an upper bound for the reconstructed mel-spectrogram.

We model the Acoustic Decoder  $\mathcal{D}^{Aco} : (s, x) \mapsto c$  as a Transformer-based model, which captures the dependencies between  $s$  and  $x$ , and decodes fMRI into the latent space of AudioMAE through a Seq2Seq generation. First, we project  $s$  and  $x$  into the 768-dimensional representation space of the Transformer. For  $s$ , we use a linear layer to project it to a semantic token  $s'$ . For  $x$ , we select 768 voxels with the highest responses based on the mapping matrix  $W$ , forming the fMRI token  $x'$ . Then we concat the tokens and encode them with a Transformer Encoder  $\mathcal{E}^T$ , obtaining the neural embedding  $n = \mathcal{E}^T([s', x'])$ . We create a learnable embedding  $q$  as the query to a Transformer Decoder  $\mathcal{D}^T$  along with  $n$  as key and value, obtaining the decoded acoustic feature  $c = \mathcal{D}^T(q, n)$ .

We train  $\mathcal{D}^{Aco}$  from scratch with three different loss functions that measure the distance between  $c$  and  $c_{gt}$ . The first one is  $\mathcal{L}_{cond}$ , which directly calculates the L2 distance in the latent space. Then, we use the AudioMAE Decoder  $\mathcal{D}^A$  to decode  $c$  into the reconstructed patches  $m_{recon}^p = \mathcal{D}^A(c)$  and unpatchify them into the mel-spectrogram  $m_{recon}$ . During the decoding process, we calculate the L2 distance between each intermediate layer representation of  $\mathcal{D}^A$  and the ground truth, which is the perceptual loss  $\mathcal{L}_{perceptual}$ . Finally, we calculate the L2 distance between  $m_{upp}$  and  $m_{recon}$  with the original mel-spectrogram  $m$  as the reconstruction loss  $\mathcal{L}_{mel}$ . The overall loss is given by:

$$\mathcal{L} = \underbrace{\|c - c_{gt}\|_2^2}_{\mathcal{L}_{cond}} + \underbrace{\sum_{i \in layer} \|\mathcal{D}_i^A(c) - \mathcal{D}_i^A(c_{gt})\|_2^2}_{\mathcal{L}_{perceptual}} + \underbrace{\|m_{upp} - m\|_2^2 + \|m_{recon} - m\|_2^2}_{\mathcal{L}_{mel}}. \quad (1)$$

Since the pretrained AudioMAE model is accustomed to working with masked patches, and our method utilizes all patches, we freeze  $\mathcal{E}^A$  and fine-tune the parameters of  $\mathcal{D}^A$  in order to achieve the best performance of reconstruction.

Furthermore, we follow Liu et al. [32] by setting a  $P_{gt} = 0.25$  during training, which means that  $\mathcal{D}^{Aco}$  has a 0.25 probability of receiving the ground truth semantic feature  $s_{gt}$  as input and a 0.75 probability of receiving the decoded semantic feature  $s$  from  $\mathcal{D}^{Sem}$ . This trick enhances the decoding performance of  $\mathcal{D}^{Aco}$  and facilitates the utilization of semantic prompts. We will discuss it in Section 3.5.

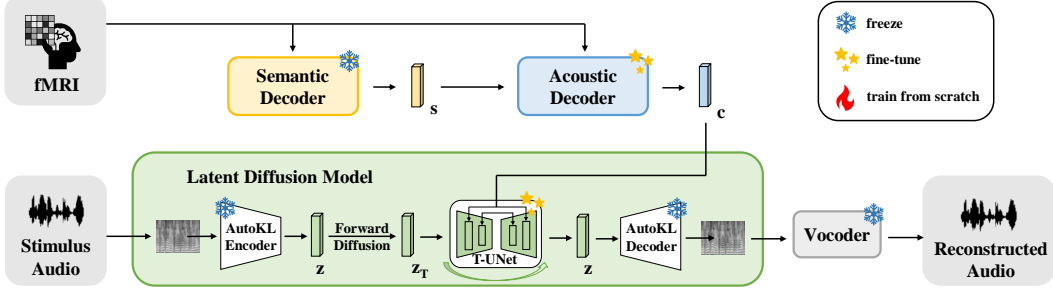


Figure 3: Brain-to-audio reconstruction. The LDM generates mel-spectrograms under the condition of fine-grained acoustic features, followed by the Vocoder to generate reconstructed audios.

## 2.2 Brain-to-audio reconstruction

In this section, we use a generative model  $\mathcal{G} : c \mapsto y$  to reconstruct the stimulus audio conditioned on  $c$ . When performing fine-grained decoding, although we use the AudioMAE Decoder to reconstruct the mel-spectrogram, it is not suitable to serve as the generative model for our method. We will discuss this in detail in Section A.4. Instead, we model the process with a Latent Diffusion Model (LDM) [28]. LDM is a powerful generative model that can model complex data distributions in the latent space. It has been extensively used in the audio generation task, such as AudioLDM [36], AudioLDM2 [32] and DiffVoice [37].

We follow the formulation in AudioLDM2 [32] to implement the LDM. As shown in Figure 3, we first use a Hanning window with 64 frequency bins, a window size of 1024, and a hop size of 160 to convert the stimulus audio into the mel-spectrogram. Then compress it to a latent representation  $z$  using a VAE. The forward diffusion process is a  $T$  steps Markov chain that gradually adds Gaussian noise as

$$q(z_t|z_{t-1}) = \mathcal{N}(z_t; \sqrt{1 - \beta_t}z_{t-1}, \beta_t\mathbf{I}) \quad (2)$$

where  $\beta_t$  is a variance schedule. Then the distribution of  $z_t$  given  $z_0$  can be formulated as

$$q(z_t|z_0) = \prod_{s=1}^t q(z_s|z_{s-1}) = \mathcal{N}(z_t; \sqrt{\alpha_t}z_0, (1 - \alpha_t)\mathbf{I}) \quad (3)$$

where  $\alpha_t = \prod_{s=1}^t (1 - \beta_s)$ . The distribution of  $z_T$  at the final step will be a standard Gaussian distribution [38]. The LDM learns a reverse denoising process from the prior distribution  $\mathcal{N}(\mathbf{0}, \mathbf{I})$  to the data distribution  $z$  conditioned on  $c$ . The loss function [28, 38] in our method can be given as

$$\mathcal{L} = \mathbb{E}_{z_t, \epsilon \sim \mathcal{N}(\mathbf{0}, \mathbf{I}), t \sim \{1, \dots, T\}} [\|\epsilon_\theta(z_t, t, c) - \epsilon\|_2^2 + \|\epsilon_\theta(z_t, t, c_{gt}) - \epsilon\|_2^2] \quad (4)$$

where  $\epsilon_\theta$  is the denoising network, for which we utilize a Transformer-UNet (T-UNet) following AudioLDM2 [32]. After the LDM reconstructs the mel-spectrogram, it will be converted to the waveform using a pretrained HiFiGAN [29] vocoder. We initialize the LDM with pretrained weights from AudioLDM2 and fine-tune  $\mathcal{D}^{Aco}$  and the T-UNet during training, while keeping other weights frozen.

## 2.3 Conditional reconstruction

In practical applications, brain-to-audio reconstruction is not always unconditional. Firstly, compared to images, audios exhibit strong temporal correlations. If a subject listens to a long segment of stimulus audio but only a portion needs to be reconstructed using brain signals, considering that other audio segments and the target segments may be semantically similar, they can serve as conditions to provide additional semantic information. Secondly, we may know in advance the coarse-grained category (e.g., human speech or animal sound) of the audio to be reconstructed. Given the challenge of semantic decoding from fMRI (see Section 3.4 for details), we can use the coarse-grained category as the semantic prior to guide the reconstruction process. Thus, we attempt to provide semantic prompts in the form of audio or text to our model for conditional reconstruction, to assess whether it can enhance the quality of the reconstructed audio.

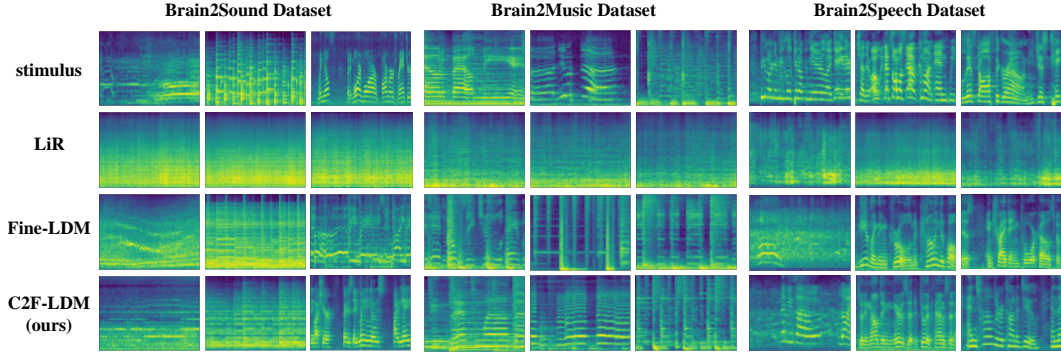


Figure 4: Reconstruction results of S1, sub-001 and UTS01 on the three datasets.

The conditional reconstruction process is straightforward. We utilize CLAP’s Text Encoder and Audio Encoder to extract the semantic embedding  $s_{prompt}$  of the text prompt and audio prompt. Then we replace  $s$  with  $s_{prompt}$  as input to  $\mathcal{D}^{Aco} : (s_{prompt}, x) \mapsto c$ , to obtain the fine-grained acoustic embedding  $c$ . Finally, we use  $\mathcal{G} : c \mapsto y$  to reconstruct the stimulus audio conditioned on  $c$ .

### 3 Experiments

#### 3.1 Datasets

We use three publicly available fMRI datasets to validate our method’s performance across different kinds of stimuli: Brain2Sound [7], Brain2Music [39], and Brain2Speech [40] datasets. Brain2Sound Dataset [7] comprises fMRI signals from five subjects listening to 4-second natural sounds, including human speech, animal, musical instrument, and environmental sounds. The dataset consists of 14,400 training samples and 150 test samples. Brain2Music Dataset [39] comprises fMRI signals from five subjects listening to 1.5-second music clips, consisting of 4,800 training samples and 600 test samples. Brain2Speech Dataset [40] comprises fMRI signals from seven subjects listening to 2-second voice segments, consisting of 9,137 training samples and 595 test samples. For detailed information about the datasets and the preprocessing methods, please refer to section A.1.

#### 3.2 Metrics

We use FD, FAD, KL, and KL-S, commonly utilized in audio generation tasks, to evaluate the quality of brain-to-audio reconstruction. FD (Fréchet Distance) calculates the distance in features between generated samples and target samples, extracted from an audio classifier PANNs [41]. KL and KL-S (Kullback–Leibler divergence) calculate the KL divergence of classification logits, also based on PANNs, using Softmax and Sigmoid activation functions respectively. FAD (Fréchet Audio Distance) is similar to FD, but it uses VGGish [42]. All metrics are implemented through the *Audio Generation Evaluation* toolbox.<sup>4</sup> The above metrics evaluate high-level representations of audio. In addition to these, we use PCC and SSIM to measure the similarity between the mel-spectrograms of reconstructed audio and stimulus audio, evaluating low-level spectrotemporal representations. Each subject conducts independent experiments, and the metrics are averaged.

#### 3.3 Reconstruction results

We compare the reconstruction results of three methods: (1) The direct decoding methods, which map fMRI signals to mel-spectrograms, including a linear regression model [8, 11–13] implemented through Ridge in sklearn, a three-layer MLP [8, 12, 13] implemented through MLPRegressor in sklearn following Bellier et al. [8], a Bidirectional LSTM [9, 14] and a Transformer Encoder [14], both with the same configuration as our Transformer. (2) The fine-grained decoding methods, which map fMRI signals to high-dimensional intermediate features directly [7, 15, 16]. We remove the coarse-grained decoding process of our method and decode fMRI into the latent space of AudioMAE

<sup>4</sup>[https://github.com/haoheliu/audioldm\\_eval](https://github.com/haoheliu/audioldm_eval)

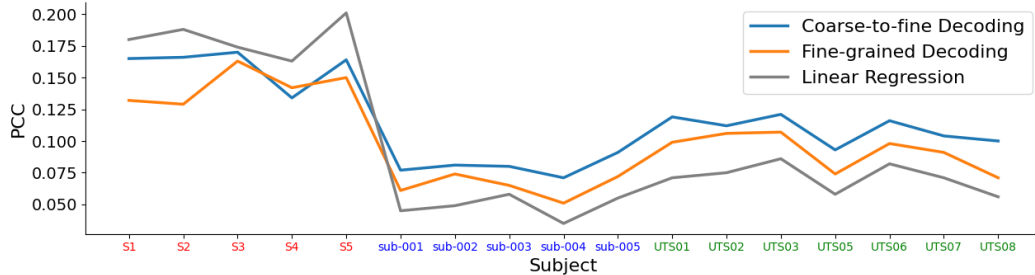


Figure 5: PCC between the ground truth and decoded acoustic features for 17 subjects in the **Brain2Sound**, **Brain2Music** and **Brain2Speech** datasets. Our coarse-to-fine method consistently outperforms the directly fine-grained method.

using the Acoustic Decoder  $\mathcal{D}^{Aco} : x \mapsto c$ . Then we used the LDM  $\mathcal{G} : c \mapsto y$  to reconstruct the audio. This method is called *Fine-LDM*. In addition, for the Brain2Sound Dataset, we use the code and checkpoints open-sourced by Park et al. [7] to reproduce their experimental results. (3) The coarse-to-fine decoding methods proposed by us, including *C2F-Decoder*, which utilizes the AudioMAE Decoder as the generative model (see details in Section A.4) and *C2F-LDM* using the LDM (ours). Please refer to section A.2 for specific details on the experimental setup.

We select one representative from each of the three methods, *Linear Regression* (*LiR*), *Fine-LDM* and *C2F-LDM*, and display the reconstructed mel-spectrograms in Figure 4. All quantitative results are displayed in Table 1. We find that direct decoding methods are able to capture the overall spectrotemporal distributions of mel-spectrograms but struggle to reconstruct details and semantics. They show high performance in low-level metrics but low performance in high-level metrics. In contrast, the fine-grained decoding methods exhibit a significant improvement in high-level metrics but a decrease in low-level metrics, which increase details in the reconstructed spectrograms. It suggests that these methods can provide a preliminary reconstruction of semantics but at the cost of losing spectrogram similarity.

Our coarse-to-fine method reconstructs the spectrogram details that are closer to the original stimulus and shows improvements in both low-level and high-level metrics compared to the fine-grained decoding methods, as shown in Figure 4 and Table 1. Although it has not yet reached the level of direct decoding methods in PCC and SSIM, it has achieved state-of-the-art performance in FD, FAD, KL, and KL-S. Compared to Park et al. [7], our method significantly improves on FD, surpasses FAD and PCC, and closely approaches the remaining metrics. The comparison of reconstructed samples can be found in Section A.3. The comparison with *C2F-Decoder* can be found in Section A.4.

We further analyze the impact of our coarse-to-fine method on decoding the fine-grained acoustic features. We compute the PCC between the ground truth and decoded acoustic features for 17

Table 1: Reconstruction results on the three datasets.

Model	PCC $\uparrow$	SSIM $\uparrow$	FD $\downarrow$	FAD $\downarrow$	KL $\downarrow$	KL-S $\downarrow$
<b>Brain2Sound Dataset [7]</b>						
LiR [8, 11–13]	<b>0.607</b>	<b>0.184</b>	105.113	40.877	4.027	9.650
MLP [8, 12, 13]	0.566	0.181	98.358	38.045	4.020	9.811
BiLSTM [9, 14]	0.526	0.134	92.172	33.442	4.187	9.668
Transformer [14]	0.526	0.132	74.048	27.526	3.817	8.974
Park et al. [7]	0.394	0.133	88.456	12.694	<b>2.251</b>	<b>6.560</b>
Fine-LDM [7, 15, 16]	0.376	0.107	49.827	10.803	2.895	7.500
C2F-Decoder	0.595	0.177	95.565	35.775	3.748	10.097
C2F-LDM (ours)	0.418	0.118	<b>44.003</b>	<b>9.324</b>	2.697	7.046
<b>Brain2Music Dataset [39]</b>						
LiR [8, 11–13]	0.637	0.197	47.710	18.247	0.997	4.105
MLP [8, 12, 13]	0.591	0.191	48.980	19.895	0.732	3.460
BiLSTM [9, 14]	0.628	<b>0.200</b>	57.030	22.673	1.008	4.117
Transformer [14]	<b>0.646</b>	0.195	60.969	22.195	1.079	4.692
Fine-LDM [7, 15, 16]	0.426	0.112	6.544	<b>1.439</b>	0.526	2.132
C2F-Decoder	0.643	0.199	63.039	26.053	1.191	4.334
C2F-LDM (ours)	0.454	0.124	<b>6.102</b>	1.504	<b>0.520</b>	<b>2.010</b>
<b>Brain2Speech Dataset [40]</b>						
LiR [8, 11–13]	0.511	0.126	68.146	24.988	3.483	8.132
MLP [8, 12, 13]	0.409	0.116	75.174	27.983	4.153	9.057
BiLSTM [9, 14]	0.580	<b>0.179</b>	112.031	39.895	3.948	10.312
Transformer [14]	<b>0.581</b>	0.173	104.118	39.484	3.764	10.228
Fine-LDM [7, 15, 16]	0.357	0.077	12.706	4.820	0.885	2.573
C2F-Decoder	0.518	0.128	96.032	26.917	4.278	9.831
C2F-LDM (ours)	0.393	0.083	<b>9.726</b>	<b>4.623</b>	<b>0.616</b>	<b>1.989</b>

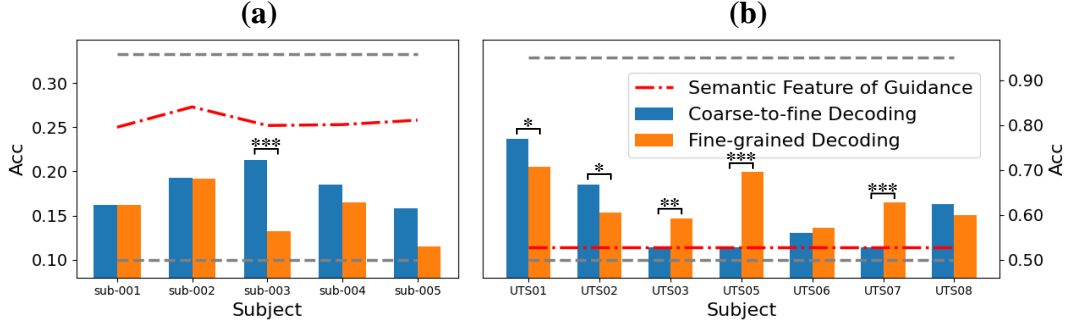


Figure 6: Semantic decoding accuracy in the (a) Brain2Music and (b) Brain2Speech Dataset. The gray dashed lines represent the upper bound of accuracy and the chance level. Significance test is performed (paired t-test,  $p < 0.001$ (\*\*\*),  $p < 0.01$ (\*\*),  $p < 0.05$ (\*)).

subjects across the three datasets. Then we compare the experimental results between the coarse-to-fine decoding and the directly fine-grained decoding, with a baseline established by directly mapping fMRI to the acoustic features using L2-regularized Linear Regression. As shown in Figure 5, the consistent decoding performance of the PCC across different methods reflects the varying signal quality of the subjects. Across almost all participants, our coarse-to-fine method consistently outperforms the fine-grained method. It suggests that coarse-to-fine decoding can effectively enhance the fine-grained acoustic features widely across the participants.

### 3.4 Semantic analysis of acoustic features

An intuitive idea is that the introduction of coarse-grained semantic decoding enhances the semantic information in the acoustic features, thereby improving the fine-grained decoding. Is this really the case? We will discuss this issue in this section.

It is generally believed that a representation space with strong semantic information exhibits the following characteristics: samples of the same category cluster in this space, while samples from different categories are far apart. Therefore, we conduct a classification experiment using two datasets with clear category labels, the Brain2Music Dataset [39] with the labels of music genres (10 classes) and the Brain2Speech Dataset [40] with the labels of speakers' genders (2 classes). We use SVM to classify the decoded acoustic features after the coarse-to-fine decoding and the directly fine-grained decoding. The experiment is conducted on the test set and the average classification accuracy using 5-fold cross-validation is used to assess the semantic information in the acoustic features. The chance levels are 0.1 and 0.5 for the two datasets, while the upper bounds are the classification accuracy on the ground truth acoustic features, which are 0.33 and 0.95.

As shown in Figure 6, after introducing the coarse-grained decoding, the classification accuracy for each subject in the Brain2Music Dataset either increases or remains essentially unchanged. However, in the Brain2Speech Dataset, the classification accuracy for some subjects decreases. It suggests that the semantic information in the acoustic features is diminishing, while the coarse-grained decoding primarily enhances the low-level acoustic information.

To explain this phenomenon, we further analyze the coarse-grained semantic features of guidance. The same SVM classification task is performed. As shown in Figure 6, the classification accuracy of the semantic features in the Brain2Music Dataset is relatively high, whereas the classification accuracy in the Brain2Speech Dataset is poor, approaching the chance level. It indicates that there is little semantic content in the semantic features, making it nearly impossible to differentiate speakers' genders. We visualize the distribution of the semantic features using t-SNE for the two datasets. As shown in Section A.5, some categories in the Brain2Music Dataset cluster well, while samples from the two categories in the Brain2Speech Dataset are mixed and almost indistinguishable, which is consistent with our experimental results. It might be because participants were more focused on listening to the content of the stories during fMRI signal collection and disregarded the speaking style of the speaker. The lack of semantic richness in the guided semantic features leads to a decrease in the semantic content of the acoustic features.



Table 2: Conditional reconstruction results with text prompts and audio prompts.

$P_{gt}$	Prompt	Brain2Music Dataset [39]						Brain2Speech Dataset [40]					
		PCC $\uparrow$	SSIM $\uparrow$	FD $\downarrow$	FAD $\downarrow$	KL $\downarrow$	KL-S $\downarrow$	PCC $\uparrow$	SSIM $\uparrow$	FD $\downarrow$	FAD $\downarrow$	KL $\downarrow$	KL-S $\downarrow$
0.0	no prompt	0.442	0.113	6.121	1.606	0.520	2.070	0.379	0.081	11.636	4.866	0.758	2.303
	text prompt	0.421	0.135	8.283	2.169	0.641	2.606	0.331	0.079	10.772	5.265	0.513	1.650
	audio prompt	-	-	-	-	-	-	0.315	0.077	7.160	4.148	0.430	1.427
0.25	no prompt	<b>0.454</b>	0.124	<b>6.102</b>	1.504	<b>0.520</b>	<b>2.010</b>	<b>0.393</b>	0.083	9.726	4.623	0.616	1.989
	text prompt	0.405	0.136	7.358	2.219	0.584	2.430	0.340	0.082	9.265	4.712	0.449	1.419
	audio prompt	-	-	-	-	-	-	0.300	0.075	7.722	4.383	0.416	1.394
0.5	no prompt	0.422	0.110	6.587	<b>1.341</b>	0.536	2.156	0.374	0.084	7.957	4.013	0.493	1.665
	text prompt	0.393	<b>0.138</b>	10.304	2.624	0.559	2.479	0.350	<b>0.089</b>	<b>6.698</b>	5.102	<b>0.348</b>	<b>1.142</b>
	audio prompt	-	-	-	-	-	-	0.303	0.076	7.129	<b>3.930</b>	0.398	1.338

In summary, although introducing the coarse-grained semantic decoding can enhance the decoding of the fine-grained acoustic features, the semantic content of the acoustic features may not be enhanced if the semantic features of guidance are poor. In such cases, the coarse-grained decoding mainly enhances the low-level acoustic information.

### 3.5 Conditional reconstruction results

From the previous section, we can see that due to the issues with the dataset, when the semantic decoding does not perform well, guidance on the acoustic decoding may worsen the semantic content of the acoustic features. Therefore, when we conduct the conditional reconstruction task mentioned in Section 2.3, it’s better to use the semantic features of prompts as the coarse-grained features instead of the decoded features. In this experiment, we define two kinds of prompts. The first one is a text prompt that includes the category of the stimulus audio. The prompts in the Brain2Music Dataset [39] consist of 10 music genres such as *pop music* and *rock music*, while the prompts in the Brain2Speech Dataset [40] include two options for the speaker’s gender: *man speaking* and *woman speaking*. The second one is an audio prompt. We utilize the last 10 stimulus audio clips from two stories in the test set as prompts for the Brain2Speech Dataset and then average the results obtained.

Since the hyperparameter  $P_{gt}$  mentioned in Section 2.1.2 is related to the input ground truth semantic feature, we attempt to evaluate the conditional brain-to-audio reconstruction with prompts under three conditions:  $P_{gt} = 0.0$ ,  $0.25$  and  $0.5$ . The results are shown in Table 2. We observe that all metrics for  $P_{gt} = 0.25$  surpass those for  $P_{gt} = 0.0$  without a prompt. For the Brain2Music Dataset, the high-level metrics are higher for  $P_{gt} = 0.25$ , while for the Brain2Speech Dataset, the high-level metrics are higher for  $P_{gt} = 0.5$ . However, on both datasets, the PCC is highest when  $P_{gt} = 0.25$ . It suggests that appropriately incorporating ground truth semantic features during training can help enhance the quality of brain-to-audio reconstruction.

For the Brain2Music Dataset, the high-level metrics decrease after incorporating the text prompts. It suggests that the text prompts of music genres we provide may not effectively represent the semantic content of the stimulus audio. After adding the text prompts, samples of the same music genre have identical coarse-grained features. Considering the relatively strong semantic decoding in the Brain2Music Dataset as mentioned in Section 3.4, the loss of the individual specificity across samples leads to a decrease in the reconstruction quality, particularly in semantics. In contrast, the semantic decoding performs poorly in the Brain2Speech Dataset, so the introduction of both text prompts and audio prompts can significantly enhance the semantics of the reconstructed audio. In summary, when coarse-grained semantic features are suboptimal, conditional reconstruction with prompts can effectively enhance the quality of the reconstructed audio.

## 4 Conclusion

In this paper, we propose a novel coarse-to-fine audio reconstruction method inspired by the hierarchical processing of the human auditory system. Our method begins by decoding fMRI data into the CLAP space to extract coarse-grained semantic features. Subsequently, leveraging these semantic features, we decode the fMRI data into the AudioMAE latent space to capture fine-grained acoustic

features. Next, we use the acoustic features as conditions to reconstruct the stimulus audio using a Latent Diffusion Model. By validating our method on three diverse fMRI datasets—Brain2Sound, Brain2Music, and Brain2Speech—our method has shown superior performance in brain-to-audio reconstruction compared to previous fine-grained methods. We have illustrated its state-of-the-art capabilities, achieving remarkable results in FD, FAD, KL, and KL-S. The integration of semantic prompts during decoding further enhances the semantics of reconstructed audio, particularly when dealing with suboptimal semantic decoding. We will discuss the limitations of our paper in Section A.6 and the broader impacts in Section A.7.

## References

- [1] Alexander JE Kell, Daniel LK Yamins, Erica N Shook, Sam V Norman-Haignere, and Josh H McDermott. A task-optimized neural network replicates human auditory behavior, predicts brain responses, and reveals a cortical processing hierarchy. *Neuron*, 98(3):630–644, 2018.
- [2] Juliette Millet, Charlotte Caucheteux, Yves Boubenec, Alexandre Gramfort, Ewan Dunbar, Christophe Pallier, Jean-Remi King, et al. Toward a realistic model of speech processing in the brain with self-supervised learning. *Advances in Neural Information Processing Systems*, 35:33428–33443, 2022.
- [3] Greta Tuckute, Jenelle Feather, Dana Boebinger, and Josh H McDermott. Many but not all deep neural network audio models capture brain responses and exhibit correspondence between model stages and brain regions. *Plos Biology*, 21(12):e3002366, 2023.
- [4] Bruno L Giordano, Michele Esposito, Giancarlo Valente, and Elia Formisano. Intermediate acoustic-to-semantic representations link behavioral and neural responses to natural sounds. *Nature Neuroscience*, 26(4):664–672, 2023.
- [5] Charlotte Caucheteux, Alexandre Gramfort, and Jean-Rémi King. Evidence of a predictive coding hierarchy in the human brain listening to speech. *Nature human behaviour*, 7(3):430–441, 2023.
- [6] Roberta Santoro, Michelle Moerel, Federico De Martino, Giancarlo Valente, Kamil Ugurbil, Essa Yacoub, and Elia Formisano. Reconstructing the spectrotemporal modulations of real-life sounds from fmri response patterns. *Proceedings of the National Academy of Sciences*, 114(18):4799–4804, 2017.
- [7] Jong-Yun Park, Mitsuaki Tsukamoto, Misato Tanaka, and Yukiyasu Kamitani. Sound reconstruction from human brain activity via a generative model with brain-like auditory features. *arXiv preprint arXiv:2306.11629*, 2023.
- [8] Ludovic Bellier, Anaïs Llorens, Déborah Marciano, Aysegul Gunduz, Gerwin Schalk, Peter Brunner, and Robert T Knight. Music can be reconstructed from human auditory cortex activity using nonlinear decoding models. *PLoS biology*, 21(8):e3002176, 2023.
- [9] Ian Daly. Neural decoding of music from the eeg. *Scientific Reports*, 13(1):624, 2023.
- [10] Timo I Denk, Yu Takagi, Takuya Matsuyama, Andrea Agostinelli, Tomoya Nakai, Christian Frank, and Shinji Nishimoto. Brain2music: Reconstructing music from human brain activity. *arXiv preprint arXiv:2307.11078*, 2023.
- [11] Brian N Pasley, Stephen V David, Nima Mesgarani, Adeen Flinker, Shihab A Shamma, Nathan E Crone, Robert T Knight, and Edward F Chang. Reconstructing speech from human auditory cortex. *PLoS biology*, 10(1):e1001251, 2012.
- [12] Minda Yang, Sameer A Sheth, Catherine A Schevon, Guy M McKhann II, and Nima Mesgarani. Speech reconstruction from human auditory cortex with deep neural networks. In *Interspeech*, pages 1121–1125, 2015.
- [13] Akbari Hassan, Bahar Khalighinejad, Jose L Herrero, Ashesh D Mehta, and Nima Mesgarani. Reconstructing intelligible speech from the human auditory cortex. *BioRxiv*, page 350124, 2018.

- [14] Kai Shigemi, Shuji Komeiji, Takumi Mitsuhashi, Yasushi Iimura, Hiroharu Suzuki, Hidenori Sugano, Koichi Shinoda, Kohei Yatabe, and Toshihisa Tanaka. Synthesizing speech from ecog with a combination of transformer-based encoder and neural vocoder. In *ICASSP 2023-2023 IEEE International Conference on Acoustics, Speech and Signal Processing (ICASSP)*, pages 1–5. IEEE, 2023.
- [15] Miseul Kim, Zhenyu Piao, Jihyun Lee, and Hong-Goo Kang. Braintalker: Low-resource brain-to-speech synthesis with transfer learning using wav2vec 2.0. In *2023 IEEE EMBS International Conference on Biomedical and Health Informatics (BHI)*, pages 1–5. IEEE, 2023.
- [16] Xupeng Chen, Ran Wang, Amirhossein Khalilian-Gourtani, Leyao Yu, Patricia Dugan, Daniel Friedman, Werner Doyle, Orrin Devinsky, Yao Wang, and Adeen Flinker. A neural speech decoding framework leveraging deep learning and speech synthesis. *Nature Machine Intelligence*, pages 1–14, 2024.
- [17] Aditya R Vaidya, Shailee Jain, and Alexander G Huth. Self-supervised models of audio effectively explain human cortical responses to speech. *arXiv preprint arXiv:2205.14252*, 2022.
- [18] Yuanning Li, Gopala K Anumanchipalli, Abdelrahman Mohamed, Peili Chen, Laurel H Carney, Junfeng Lu, Jinsong Wu, and Edward F Chang. Dissecting neural computations in the human auditory pathway using deep neural networks for speech. *Nature Neuroscience*, 26(12):2213–2225, 2023.
- [19] Wendy A de Heer, Alexander G Huth, Thomas L Griffiths, Jack L Gallant, and Frédéric E Theunissen. The hierarchical cortical organization of human speech processing. *Journal of Neuroscience*, 37(27):6539–6557, 2017.
- [20] Josef P Rauschecker and Biao Tian. Mechanisms and streams for processing of “what” and “where” in auditory cortex. *Proceedings of the National Academy of Sciences*, 97(22):11800–11806, 2000.
- [21] Jon H Kaas and Troy A Hackett. Subdivisions of auditory cortex and processing streams in primates. *Proceedings of the National Academy of Sciences*, 97(22):11793–11799, 2000.
- [22] Sophie K Scott and Ingrid S Johnsrude. The neuroanatomical and functional organization of speech perception. *Trends in neurosciences*, 26(2):100–107, 2003.
- [23] Gregory Hickok and David Poeppel. The cortical organization of speech processing. *Nature reviews neuroscience*, 8(5):393–402, 2007.
- [24] Josef P Rauschecker and Sophie K Scott. Maps and streams in the auditory cortex: nonhuman primates illuminate human speech processing. *Nature neuroscience*, 12(6):718–724, 2009.
- [25] Umut Güçlü, Jordy Thielen, Michael Hanke, and Marcel Van Gerven. Brains on beats. *Advances in Neural Information Processing Systems*, 29, 2016.
- [26] Yusong Wu, Ke Chen, Tianyu Zhang, Yuchen Hui, Taylor Berg-Kirkpatrick, and Shlomo Dubnov. Large-scale contrastive language-audio pretraining with feature fusion and keyword-to-caption augmentation. In *ICASSP 2023-2023 IEEE International Conference on Acoustics, Speech and Signal Processing (ICASSP)*, pages 1–5. IEEE, 2023.
- [27] Po-Yao Huang, Hu Xu, Juncheng Li, Alexei Baevski, Michael Auli, Wojciech Galuba, Florian Metze, and Christoph Feichtenhofer. Masked autoencoders that listen. *Advances in Neural Information Processing Systems*, 35:28708–28720, 2022.
- [28] Robin Rombach, Andreas Blattmann, Dominik Lorenz, Patrick Esser, and Björn Ommer. High-resolution image synthesis with latent diffusion models. In *Proceedings of the IEEE/CVF conference on computer vision and pattern recognition*, pages 10684–10695, 2022.
- [29] Jungil Kong, Jaehyeon Kim, and Jaekyoung Bae. Hifi-gan: Generative adversarial networks for efficient and high fidelity speech synthesis. *Advances in neural information processing systems*, 33:17022–17033, 2020.

- [30] Vladimir Iashin and Esa Rahtu. Taming visually guided sound generation. *arXiv preprint arXiv:2110.08791*, 2021.
- [31] Alexei Baevski, Yuhao Zhou, Abdelrahman Mohamed, and Michael Auli. wav2vec 2.0: A framework for self-supervised learning of speech representations. *Advances in neural information processing systems*, 33:12449–12460, 2020.
- [32] Haohe Liu, Qiao Tian, Yi Yuan, Xubo Liu, Xinhao Mei, Qiuqiang Kong, Yuping Wang, Wenwu Wang, Yuxuan Wang, and Mark D Plumbley. Audioldm 2: Learning holistic audio generation with self-supervised pretraining. *arXiv preprint arXiv:2308.05734*, 2023.
- [33] Jort F Gemmeke, Daniel PW Ellis, Dylan Freedman, Aren Jansen, Wade Lawrence, R Channing Moore, Manoj Plakal, and Marvin Ritter. Audio set: An ontology and human-labeled dataset for audio events. In *2017 IEEE international conference on acoustics, speech and signal processing (ICASSP)*, pages 776–780. IEEE, 2017.
- [34] Andrea Agostinelli, Timo I Denk, Zalán Borsos, Jesse Engel, Mauro Verzetti, Antoine Caillon, Qingqing Huang, Aren Jansen, Adam Roberts, Marco Tagliasacchi, et al. MusiclM: Generating music from text. *arXiv preprint arXiv:2301.11325*, 2023.
- [35] Daniel Povey, Arnab Ghoshal, Gilles Boulianne, Lukas Burget, Ondrej Glembek, Nagendra Goel, Mirko Hannemann, Petr Motlicek, Yanmin Qian, Petr Schwarz, et al. The kaldI speech recognition toolkit. In *IEEE 2011 workshop on automatic speech recognition and understanding*. IEEE Signal Processing Society, 2011.
- [36] Haohe Liu, Zehua Chen, Yi Yuan, Xinhao Mei, Xubo Liu, Danilo Mandic, Wenwu Wang, and Mark D Plumbley. Audioldm: Text-to-audio generation with latent diffusion models. *arXiv preprint arXiv:2301.12503*, 2023.
- [37] Zhijun Liu, Yiwei Guo, and Kai Yu. Diffvoice: Text-to-speech with latent diffusion. In *ICASSP 2023-2023 IEEE International Conference on Acoustics, Speech and Signal Processing (ICASSP)*, pages 1–5. IEEE, 2023.
- [38] Jonathan Ho, Ajay Jain, and Pieter Abbeel. Denoising diffusion probabilistic models. *Advances in neural information processing systems*, 33:6840–6851, 2020.
- [39] Tomoya Nakai, Naoko Koide-Majima, and Shinji Nishimoto. Music genre neuroimaging dataset. *Data in Brief*, 40:107675, 2022.
- [40] Amanda LeBel, Lauren Wagner, Shailee Jain, Aneesh Adhikari-Desai, Bhavin Gupta, Allyson Morgenthal, Jerry Tang, Lixiang Xu, and Alexander G Huth. A natural language fmri dataset for voxelwise encoding models. *Scientific Data*, 10(1):555, 2023.
- [41] Qiuqiang Kong, Yin Cao, Turab Iqbal, Yuxuan Wang, Wenwu Wang, and Mark D Plumbley. Panns: Large-scale pretrained audio neural networks for audio pattern recognition. *IEEE/ACM Transactions on Audio, Speech, and Language Processing*, 28:2880–2894, 2020.
- [42] Kevin Kilgour, Mauricio Zuluaga, Dominik Roblek, and Matthew Sharifi. Fréchet audio distance: A metric for evaluating music enhancement algorithms. *arXiv preprint arXiv:1812.08466*, 2018.
- [43] Honglie Chen, Weidi Xie, Andrea Vedaldi, and Andrew Zisserman. Vggsound: A large-scale audio-visual dataset. In *ICASSP 2020-2020 IEEE International Conference on Acoustics, Speech and Signal Processing (ICASSP)*, pages 721–725. IEEE, 2020.
- [44] George Tzanetakis and Perry Cook. Musical genre classification of audio signals. *IEEE Transactions on speech and audio processing*, 10(5):293–302, 2002.
- [45] Ilya Loshchilov and Frank Hutter. Decoupled weight decay regularization. *arXiv preprint arXiv:1711.05101*, 2017.

## A Appendix

### A.1 Datasets

Table 3: ROIs and voxels of the datasets.

Dataset	ROIs	Subjects	Voxels	Training samples	Test samples
Brain2Sound [7]	AC (A1, LBelt, A4, A5, etc.)	S1	6,662	13,872	150
		S2	6,624	13,944	
		S3	6,713	13,944	
		S4	6,157	13,944	
		S5	7,143	13,944	
Brain2Music [39]	N/A	sub-001	60,784	4,800	600
		sub-002	53,927		
		sub-003	64,700		
		sub-004	61,899		
		sub-005	53,421		
Brain2Speech [40]	AC, FFA, OFA, PPA, etc.	UTS01	836	9,137	595
		UTS02	2,093		
		UTS03	1,303		
		UTS05	920		
		UTS06	980		
		UTS07	1,584		
		UTS08	1,109		

**Brain2Sound Dataset** As proposed by Park et al. [7], this dataset<sup>5</sup> records the fMRI signals of five subjects (one female) while they are listening to natural sounds, including human speech, animal, musical instrument, and environmental sounds. fMRI data are acquired using a 3.0-Tesla Siemens MAGNETOM Verio scanner at the Kyoto University Institute for the Future of Human Society. Functional images that cover the entire brain are obtained with TR = 2,000 ms, TE = 44.8 ms, flip angle = 70 deg, FOV = 192 × 192 mm, voxel size = 2 × 2 × 2 mm, number of slices = 76 and multi-band factor = 4.

The stimuli consist of 1,250 8-s natural sound segments, with 1,200 for the training set and 50 for the test set, selected from the *VGGSound dataset* [43]. All the sounds are extracted from the videos uploaded to YouTube. To increase the sample number, we preprocess the audio segments in the same way as Park et al. [7]: 4-s sliding windows are utilized with a 2-s stride to extract 3 4-s segments. All audio clips are resampled to 16kHz. During the collection of fMRI signals, each stimulus is repeated four times, resulting in 14,400 samples<sup>6</sup> for the training set (1,200 stimuli × 4 repetitions × 3 samples = 14,400 samples). For the test set, we average the multiple fMRI samples, resulting in 150 samples (50 stimuli × 3 samples = 150 samples).

**Brain2Music Dataset** Following Denk et al. [10], we use the *music genre neuroimaging dataset*<sup>7</sup> from Nakai et al. [39], which records the fMRI signals of five subjects (two female) while they are listening to music clips. fMRI data are acquired using a 3.0T MRI scanner (TIM Trio; Siemens, Erlangen, Germany) at the Center for Information and Neural Networks (CiNet), National Institute of Information and Communications Technology (NICT), Osaka, Japan. Functional scanning is performed with TR = 1,500 ms, TE = 30 ms, flip angle = 62 deg, FOV = 192 × 192 mm, voxel size = 2 × 2 × 2 mm and multi-band factor = 4.

The dataset contains music stimuli from 10 genres (blues, classical, country, disco, hip-hop, jazz, metal, pop, reggae, and rock) which are sampled from the *GTZAN dataset* [44]. A total of 54 15-s music pieces are selected from each genre, with 48 for the training set and 6 for the test set. All music pieces are resampled to 16kHz and segmented into 10 clips of 1.5 seconds each to match the TR of

<sup>5</sup><https://github.com/KamitaniLab/SoundReconstruction>

<sup>6</sup>When downloading, we discovered that some audios in the training set were no longer available on YouTube, hence, the amount of training samples is slightly less than 14,400. See Table 3 for details.

<sup>7</sup><https://openneuro.org/datasets/ds003720>

functional scanning. As a result, the dataset consists of 4,800 samples ( $48 \text{ stimuli} \times 10 \text{ genres} \times 10 \text{ samples} = 4,800 \text{ samples}$ ) for training and 600 ( $6 \text{ stimuli} \times 10 \text{ genres} \times 10 \text{ samples} = 600 \text{ samples}$ ) for testing.

**Brain2Speech Dataset** We use the dataset<sup>8</sup> proposed by LeBel et al. [40]. The dataset contains fMRI responses recorded while 7 participants<sup>9</sup> (three female) are listening to 27 complete, natural, narrative stories. fMRI data are collected on a 3T Siemens Skyra scanner at the UT Austin Biomedical Imaging Center. Functional scans are collected with TR = 2.00 s, TE = 30.8 ms, flip angle = 71 deg, multi-band factor = 2, voxel size =  $2.6 \times 2.6 \times 2.6 \text{ mm}$  and FOV = 220 mm.

The stimulus set consists of 27 10–15 minute stories from *The Moth* podcast. We select two stories (*Hang time* by a male speaker and *Where there’s Smoke* by a female speaker) as the test set, and the remaining 25 stories are used as the training set. All stories are resampled to 16kHz and segmented into 2-s clips to match the TR of functional scanning. To account for the hemodynamic response, we form a sample pair by combining the fMRI signal of each TR with the stimulus audio clip from 4 seconds ago. We use the last 10 stimulus audio clips from two stories in the test set as audio prompts. These prompts are not used for testing, ensuring that the participants could not have possibly heard the audio prompts in the preceding trials. As a result, the dataset consists of 9,137 samples for training and 595 samples for testing per subject.

## A.2 Experimental setup

In the stage of coarse-grained decoding, for the Brain2Sound and Brain2Speech datasets, we only utilize voxels from the auditory cortex (AC) area, whereas for the Brain2Music Dataset, we use voxels from the entire brain. The specific brain regions and voxels can be found in Table 3.

In the stage of fine-grained decoding, we utilize a 4-layer Transformer Encoder and Decoder in  $\mathcal{D}^{Aco}$  and initialize AudioMAE with the pretrained weights.<sup>10</sup> Since the pretrained AudioMAE requires 10-second audios ( $128 \times 1024 \text{ mel-spectrograms}$ ) as inputs, we duplicate the stimulus waveforms to 10 seconds. After encoding with the AudioMAE Encoder  $\mathcal{E}^A$ , we select the embeddings of the first  $N_{patch}$  patches as  $c_{gt}$ , corresponding to the length of the stimulus audio. We set  $N_{patch} = 208$  for the Brain2Sound Dataset,  $N_{patch} = 80$  for the Brain2Music Dataset, and  $N_{patch} = 112$  for the Brain2Speech Dataset.

In the stage of brain-to-audio reconstruction, we utilize two checkpoints of AudioLDM2<sup>11</sup> as the initialization weights for our LDM  $\mathcal{G}$ : *audioldm2-full* for the Brain2Sound and Brain2Music datasets, and *audioldm2-speech-gigaspeech* for the Brain2Speech dataset.

We use the AdamW [45] optimizer to train  $\mathcal{D}^{Aco}$  and  $\mathcal{D}^A$  with a learning rate of  $1e-6$ , and train  $\mathcal{G}$  with a learning rate of  $1e-4$ . All training is completed on a single NVIDIA A100 80GB GPU.

## A.3 Comparison with Park et al.

We reproduce the experimental results of Park et al. [7] using the features from the conv5\_3 layer of VGGish-ish [30] and voxels from the entire AC region, and compare them with our method.

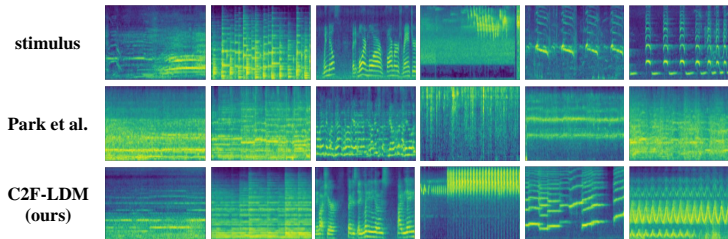


Figure 7: Comparison with the reconstruction results of Park et al. [7].

<sup>8</sup><https://openneuro.org/datasets/ds003020/versions/1.1.1>

<sup>9</sup>Subject UTS04 lacks a story, hence it will not be utilized.

<sup>10</sup><https://github.com/facebookresearch/AudioMAE>

<sup>11</sup><https://github.com/haoheliu/AudioLDM2>

#### A.4 C2F-Decoder vs. C2F-LDM

When performing fine-grained decoding, although we use the AudioMAE Decoder to reconstruct the mel-spectrogram, it is not suitable to serve as the generative model for our method. There are two main reasons for this: (1) The mel bins and window parameters of the mel-spectrograms in AudioMAE do not align with those of commonly used pretrained Vocoders. This mismatch prevents the generated mel-spectrograms from being directly converted into audio. Moreover, the cost of training a compatible Vocoder from scratch is prohibitively high. (2) The primary task of the AudioMAE Decoder is to predict masked patches, with a focus on low-level details of the spectrogram. This limitation leads to insufficient reconstruction quality in terms of semantic content. In contrast, the mel-spectrograms generated by LDM can be directly restored to audio using the pretrained HiFiGAN [29] vocoder, and the generated audio has richer semantic and acoustic details.

To investigate the reconstruction performance of *C2F-Decoder*, we need to transform the mel-spectrograms generated by the AudioMAE Decoder, denoted as  $m^A$ , into mel-spectrograms that the Vocoder can accept, denoted as  $m^V$ . We assume that  $m^A$  and  $m^V$  have a linear relationship, so we use an L2-regularized linear regression model trained on  $m^A$  and  $m^V$  of the stimulus audio in the training set. The results in the test set are as follows: PCC = 0.938 in the Brain2Sound Dataset, PCC = 0.967 in the Brain2Music and Brain2Speech datasets. Based on the results, we believe that this transformation is almost lossless. As shown in Figure 8 and Table 1, *C2F-Decoder* is similar to the direct decoding methods in that they both focus on modeling the overall spectrogram but lack detail and semantic information compared to *C2F-LDM*.

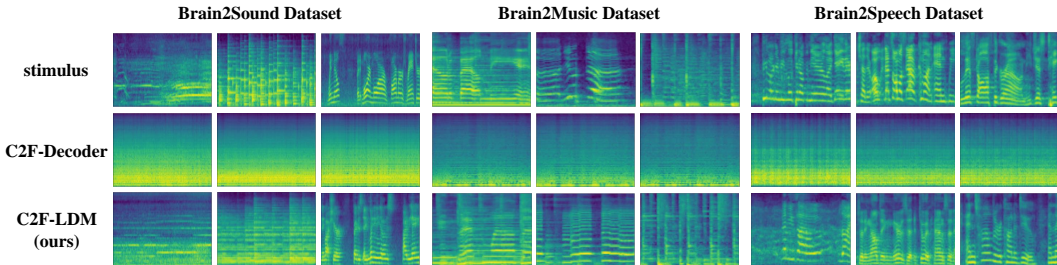


Figure 8: Comparison of the reconstruction results between *C2F-Decoder* and *C2F-LDM*.

#### A.5 Coarse-grained semantic decoding

We perform t-SNE visualization on the space of ground truth and decoded semantic features on the Brain2Music and Brain2Speech datasets. We choose the decoding spaces of sub-003 and UTS05, which show significant effects after incorporating the semantic features based on Figure 6. For the Brain2Music Dataset, some genres like *classical* and *jazz* exhibit good decoding performance, while others like *rock* show poor decoding performance, as shown in Figure 9. For the Brain2Speech Dataset, the semantic decoding performance is poor, and it cannot differentiate between male and female speakers, as shown in Figure 10.

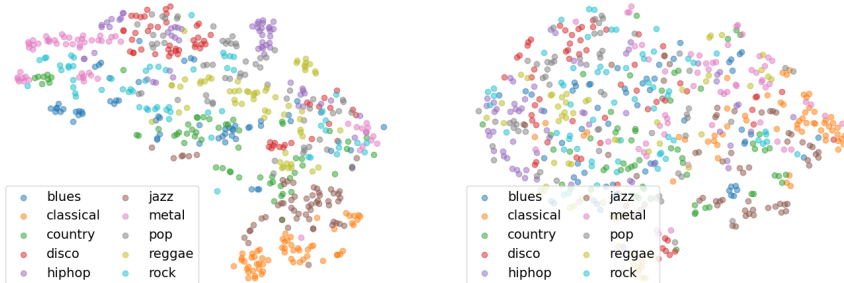


Figure 9: Visualization on the space of ground truth (left) and decoded (right) semantic features on the Brain2Music Dataset.



Figure 10: Visualization on the space of ground truth (left) and decoded (right) semantic features on the Brain2Speech Dataset. The cross markers represent samples used as audio prompts, providing coarse-grained semantic features in the conditional reconstruction.

### A.6 Limitations and future work

The main purpose of this article is to illustrate the superiority of hierarchical decoding over direct decoding. Therefore, we build a generic brain-to-audio framework, selecting the most suitable models, CLAP and AudioMAE, without comparing them to other representation models. In the future, we will switch to different models within our framework to attempt further improvement of reconstruction results. Furthermore, we utilize all the voxels of the auditory cortex (AC) in our work. However, there are gradients in the voxels of different brain regions within the AC. In the future, we plan to consider the gradients of voxels to further enhance the hierarchy of information processing.

### A.7 Broader Impacts

This research contributes to enhancing our understanding of brain function and cognitive processes, playing a crucial role in further exploring the mechanisms of the human auditory system and promoting the development of related technologies. The experiments are conducted in a controlled laboratory setting with the participants' consent and cooperation. It is not applicable in real-world scenarios, thereby posing a minimal risk of privacy leakage.